Accelerated Bayesian Searches for Gravitational Waves from Eccentric Binary Systems

Gabriel E. Freedman
Department of Physics, University of Wisconsin-Milwaukee
Milwaukee, WI, USA

Abstract

Pulsar timing arrays (PTAs) can detect low-frequency gravitational waves (GWs) by searching for correlations in the residuals of pulse arrival times. Among the many interesting sources of these GWs are individual supermassive black hole binaries (SMBHBs). Performing a full Bayesian inference of individual GW sources with PTA data is a computationally intensive and often prohibitive task due to the large parameter spaces, complicated deterministic signal modeling, and parameter covariances. Recently methods have been developed to speed up the analysis of GWs from circular SMBHBs by separating the parameter space in shape and projection parameters, and effectively marginalizing over parameters whose updates incur very little computational cost in the model likelihood. We extend these methods to a pipeline for eccentric SMBHB sources, and present its accuracy in recovering GW signal parameters in simulated data. We also test the scalability of this method to future larger datasets, and discuss what changes can be made for future analyses.

1. Introduction

The discovery of a low-frequency stochastic gravitational wave (GW) signal by the North American Nanohertz Observatory for Gravitational Waves (Agazie et al. 2023c), European Pulsar Timing Array (Antoniadis et al. 2023), and Parkes Pulsar Timing Array (Reardon et al. 2023) has opened a new chapter in the field of GW astrophysics. Pulsar timing array (PTAs; Sazhin 1978; Detweiler 1979; Foster & Backer 1990) collaborations search for nHz frequency GWs by analyzing the the times-of-arrival (TOA) in radio pulses emitted by millisecond pulsars. By regularly observing such pulsars over a decades-long timespan PTAs can reach the sensitivity necessary to probe the nHz band. The recently identified stochastic GW signal displayed, to varying levels of significance, the expected Hellings-Downs (HD; Hellings & Downs 1983) spatial correlations between pulsars that is indicative of the signal being a gravitational wave background (GWB).

The nHz GWB is typically described as the collective signal from the population of supermassive black hole binaries (SMBHB) present in the observable universe (Sesana et al. 2005). All massive galaxies hold a supermassive black hole, typically of mass $10^6 - 10^{10} M_\odot$, at their centers (Kormendy & Ho 2013). Galactic merger events consequently lead to the formation of SMBHB systems. When the component black holes reach inspiral phase, the emission of GWs becomes the dominant force behind the system's evolution. To date there have been no confirmed observations of SMBHBs. With the discovery of a GWB signal, a next major step for PTA science is to search for particularly loud individual binaries that can be detected amongst the stochastic ensemble. Measurements of GWs from individual sources would provide useful constraints on the astrophysical environments of SMBHBs (Quinlan 1996; Haiman et al. 2009) and could be coupled with electromagnetic observations to study galactic evolution and further multimessenger astrophysical research (eg. Charisi et al. 2022).

Many previous analyses have been carried out using PTA data aiming to detect and characterize GWs from single binaries, and they have placed progressively more stringent upper limits as the data set sensitivity grows (Arzoumanian et al. 2023). In practice, Bayesian methods to conduct these searches tend to be computationally intensive and inefficient undertakings, where the Markov Chain Monte Carlo methods working under the hood struggle to sample with large parameter spaces and the irregularly sampled TOA data that requires PTA GW searches to exist entirely in the time domain. Furthermore, these analyses are often restricted to the case of circular orbits, as over time GW emission will cause the binary to circularize. However, it has been shown that binary systems can retain significant eccentricities when reaching the sensitivity of the PTA band, and therefore a more complete prescription for analyzing the more complex eccentric signal model is necessary (eg. Armitage & Natarajan 2005; Roedig & Sesana 2012).

Recently new analysis techniques have been developed in the code `QuickCW` (Bécsy et al. 2022) that offer a speed-up of roughly two orders of magnitude for the individual circular binary search. This is accomplished by dividing the model space into two classes: *projection* parameters that determine how a GW signal is projected onto the lines-of-sight of the pulsars, and *shape* parameters that define the morphology and structure of the signal itself. In this paper we propose an extension to the `QuickCW` algorithm to account for eccentric binary orbits and their evolution, and evaluate the potential for a generalized individual binary search with current PTA data.

This paper is organized as follows. In Sec. 2 we outline the signal models for the individual binary GW search and define the reformulated likelihood function and other improvements to the Bayesian analysis pipeline. We analyze simulated data sets in Sec. 3 and scale the computational efficiency of the new method against future data volume increases. We conclude in Sec. 4 and discuss future directions of this research. In this paper we use units where $G = c = 1$.

2. Methods

In this paper we focus solely on the Bayesian methods used to carry out GW analyses. This is a method of statistical inference in which one's knowledge of an event is updated with subsequent observations, and the term "probability" refers to the degree of belief in a particular event. A standard way to perform such inference is through Markov Chain Monte Carlo (MCMC) sampling, where samples of the target posterior distribution are iteratively drawn according to some proposal distributions and accepted or rejected according to a pre-defined algorithm such as the Metropolis-Hastings condition (Metropolis et al. 1953).

We describe the data acquisition, preprocessing, and noise modeling in Sec. 2.1. In Sec. 2.2 we outline the signal models for individual binary sources in both circular and eccentric orbits. We then define a reformulated model likelihood in Sec. 2.3 that allows for faster evaluation of specific sets of parameters. Lastly in Sec. 2.4 we introduce a modified MCMC algorithm that can best leverage the new likelihood and parameter groupings.

2.1. PTA Data and Noise Model Pulsars are observed using the Arecibo Observatory, the Green Bank Telescope, and the Very Large Array, with measurements taken in frequencies ranging from 327 MHz to 3GHz. Observational cadences, or "epochs" are typically on the order of once per month. Data acquisition systems produce pulse profiles from raw baseband data by performing coherent dedispersion, RFI excision, flux calibration, and polarization calibration. Time-of-arrival (TOA) data are then generated from the profiles using the `PSRCHIVE` package. The processed TOAs are then fit on a per-pulsar basis to a timing model comprising pulsar-specific parameters such as sky locaiton, parallax, spin period and spin period derivative. For binary pulsars, this also includes five Keplerian binary parameters. The fits are conducted using the `TEMPO2` and `PINT` packages.

We model the timing residuals as a linear combination of noise sources and potential GW signals, denoted as:

$$\delta t = M\varepsilon + n_{\text{WN}} + n_{\text{RN}} + n_{\text{CURN}} + s. \tag{1}$$

The term $M\varepsilon$ represents errors inherit to the timing model, with M being the design matrix describing the linearized model and ε offsets from the model parameters. The terms n_{WN} and n_{RN} describe the per-pulsar white- and red-noise contributions, respectively. Spatially correlated red-noise signals that are common amongst all pulsars are included as n_{CURN}. Lastly, s defines the induced timing delay originating from deterministic sources, such as GWs from individual binaries. For a more complete review of PTA noise modeling, we direct the reader to Agazie et al. (2023b).

At the heart of any MCMC sampler for Bayesian inference is repeated calculations of the model (log-)likelihood, which for the timing residuals defined above can be written as:

$$\log L = -\frac{1}{2}\left(\delta t - s|\delta t - s\right) - \frac{1}{2}\log\det\left(2\pi C\right), \tag{2}$$

where the inner products are defined as $(a|b) = a^T C^{-1} b$. Here C is the total covariance matrix for the model, created as a combination of the white noise covariance matrix N, the design matrix T, and the hyperparameter prior matrix B, written as $C = N + TBT^T$.

2.2. Continuous Gravitational Wave Sources We now review the signal model for GWs originating from an SMBHB and their effect on PTA residuals. The GW signal, often called a continuous wave, or CW, due to its minimal frequency evolution, can be written as (for a detailed review, see Arzoumanian et al. 2023):

$$s(t, \hat{\Omega}) = F^{+}(\theta, \phi, \psi)\Delta s_{+}(t) + F^{\times}(\theta, \phi, \psi)\Delta s_{\times}(t), \tag{3}$$

where the scripts $\{+\times\}$ denote the plus and cross polarization modes, the two tensor polarizations allowed by general relativity. The functions F^{+} and $F^{\times}$ represent the antenna pattern functions that describe the response of a given pulsar to the emitting source, and are composed of the binary sky location parameters (θ, ϕ) and GW polarization angle (ψ). The terms $\Delta s_{+,\times}(t)$ account for the fact that the Earth and pulsar see the induced GW signal at different times in the binary evolution, and therefore define the difference between the "pulsar-term" and "Earth-term":

$$\Delta s_{+,\times}(t) = s_{+,\times}(t_p) - s_{+,\times}(t), \tag{4}$$

where t_p is the time measured at the pulsar and t the time measured at the solar system barycenter. The exact forms of $s_{+,\times}(t)$ for a circular binary are given, to zeroth Post-Newtonian (0-PN) order, by:

$$s_{+}(t) = -\frac{\mathcal{M}^{5/3}}{d_L \omega(t)^{1/3}} \sin 2\Phi(t) \left(1 + cos^2 \imath\right), \quad s_{\times}(t) = \frac{\mathcal{M}^{5/3}}{d_L \omega(t)^{1/3}} 2 \cos 2\Phi(t) \cos \imath. \tag{5}$$

The parameter $\mathcal{M}$ represents the binary chirp mass $\mathcal{M} \equiv (m_1 m_2)^{3/5}/(m_1 + m_2)^{1/5}$ for the component black hole masses m_1 and m_2. The parameters d_L and $\imath$ are the luminosity distance to the binary and the source inclination angle, respectively. The time-dependent angular frequency and phase functions are, for reference Earth-term frequency ω_0 and phase Φ_0:

$$\omega(t) = \omega_0 \left[1 - \frac{256}{5} \mathcal{M}^{5/3} \omega_0^{8/3} (t - t_0)\right]^{-3/8} \tag{6}$$

$$\Phi(t) = \Phi_0 + \frac{1}{32} \mathcal{M}^{-5/3} \left[\omega_0^{-5/3} - \omega(t)^{-5/3}\right]. \tag{7}$$

Circular CW signals have the benefit that they can be written in succinct analytical form through the equations given above. However, they do not give a complete picture of the SMBHB population as in general binaries will have a, perhaps non-negligible, non-zero eccentricity. The inclusion of binary eccentricity and the evolution of its orbit complicates the signal model considerably. For a complete derivation of the GW waveforms for eccentric binary orbits we direct the reader to Peters (1964), and for a full details of the signal induced by SMBHBs on PTA data see Taylor et al. (2016) and Susobhanan et al. (2020). Below we summarize the relevant details.

First we note the additional parameters necessary for describing the evolution of eccentric orbits. In addition to the binary eccentricity, e, there are a number of new angular parameters. There is the eccentric anomaly, u, which serves to parameterize the radial and phase coordinates. There is the mean anomaly, l, directly related as $l = u - e \sin u$. The true anomaly, Φ, is the direct analog of the standard phase coordinate. And we also must include the angle of periapsis, γ, in our derivations. Unlike the circular case, the orbital frequency is no longer constant and instead the CWs are emitted across a range of frequencies. In order to account for this, our focus shifts to the mean orbital frequency, F.

With these changes in mind, the PTA residuals induced by the eccentric CW can be written, as shown in Taylor et al. (2016), as:

$$\begin{aligned} s_+(t) &= \sum_n -\left(1+\cos^2\imath\right)\left[a_n\cos(2\gamma) - b_n\sin(2\gamma)\right] + \left(1-\cos^2\imath\right)c_n \\ s_\times(t) &= \sum_n 2\cos\imath\left[b_n\cos(2\gamma) + a_n\sin(2\gamma)\right], \end{aligned} \tag{8}$$

where the coefficients a_n, b_n, and c_n are:

$$\begin{aligned} a_n &= -\zeta\omega^{-1/3}\left[J_{n-2}(ne) - 2eJ_{n-1}(ne) + (2/n)J_n(ne) + 2eJ_{n+1}(ne) - J_{n+2}(ne)\right]\sin[nl(t)] \\ b_n &= \zeta\omega^{-1/3}\sqrt{1-e^2}\left[J_{n-2}(ne) - 2J_n(ne) + J_{n+2}(ne)\right]\cos[nl(t)] \\ c_n &= (2/n)\zeta\omega^{-1/3}J_n(ne)\sin[nl(t)]. \end{aligned} \tag{9}$$

with ζ defined as an amplitude parameter $\zeta \equiv \mathcal{M}^{5/3}/d_L$ and $\omega = 2\pi F$. As expected from the harmonic structure of GW emission from such orbits, the expression for the induced signal is dominated by Bessel functions. Add to this the fact that expressing PN-accurate models requires solving coupled differential equations for n, e, γ, and l to fully model their time evolution, and the computational limitations of analyzing deterministic CW signals becomes clear.

2.3. Reformulated CW Likelihood The problem of dealing with large correlated parameter spaces with costly likelihood evaluations has been alleviated for the case of circular CWs through work developed in Bécsy et al. (2022). Similar to the $\mathcal{F}$-statistic methods described in Ellis et al. (2012), one can separate the CW parameter space into shape $\boldsymbol{\theta}_s = \{\theta, \phi, \omega_0, \mathcal{M}\}$ and projection $\boldsymbol{\theta}_p = \{\imath, d_L, \psi, \Phi_0\}$ parameters. This allows Eq. 5 to be written as:

$$s(t, \hat{\Omega}) = \sum_{j=1}^{4} \sigma_{4(i-1)+j}\left(\theta, \phi, \imath, \psi, \Phi_0\right) S^{4(i-1)+j}(t) \tag{10}$$

dividing it into a set of filter functions $S^k(t)$ and coefficients σ_k given by Eqs. (15) and (18), respectively, in Bécsy et al. (2022). Using this set of filters and coefficients allows for a reformulation of Eq. 2 to:

$$\log L = -\frac{1}{2}\left(\delta t|\delta t\right) - \frac{1}{2}\log\det\left(2\pi C\right) + \sum_{k=1}^{4N_p}\sigma_k N^k - \frac{1}{2}\sum_{k=1}^{4N_p}\sum_{l=1}^{4N_p}\sigma_k\sigma_l M^{kl}, \tag{11}$$

where N_p refers to the number of pulsars in the array, $M^{kl} = (S^k|S^l)$, and $N^k = (\delta t|S^k)$. The most expensive part of calculating this likelihood is the evaluation of the inner products M^{kl} and N^k, which depend entirely on the shape parameters. Therefore, evaluating Eq. 11 for any set of projection parameters, with all other parameters held fixed, can be done nearly instantly.

2.4. Multiple-Try Markov Chain Monte Carlo For a standard MCMC routine, the computational burden is spread equally across the model; all parameters are updated once at a time and simultaneously. In the order to take full advantage of the new form of the CW likelihood, it is necessary to use an MCMC routine that will perform a large number of updates to projection parameters for every single update of shape parameters. This is accomplished using the Multiple-Try Markov Chain Monte Carlo (MTMCMC; Liu et al. 2000) routine, outlined in Algorithm 1, which serves to maximize the mixing of model parameters that are separated into multiple classes.

In the instance of the CW likelihood, MTMCMC operates by drawing some large block (typically $n \sim \mathcal{O}(10^3)$) of projection parameter updates for a single set of shape parameters. They are drawn according to some joint proposal

Algorithm 1 Multiple-Try Markov Chain Monte Carlo

Require: $\mathbf{x}$, M, N
  for $t = 1...M$ **do**
    Draw $\mathbf{y}_1...\mathbf{y}_N \sim Q(\mathbf{x}, .)$
    for $j = 1...N$ **do**
      Compute $L(\mathbf{x}, \mathbf{y}_j)$
    end for
    According to probability mass function $p(\mathbf{x}, \mathbf{y}) = \frac{L(\mathbf{x},\mathbf{y})}{\sum_{k=1}^{N} L(\mathbf{x},\mathbf{y})}$, select $\mathbf{y} \in \mathbf{y}_i$
    Draw $\mathbf{x}_1...\mathbf{x}_{k-1} \sim Q(., \mathbf{y})$, set $\mathbf{x}_k \leftarrow \mathbf{x}$
    With probability $\alpha = \min\left\{1, \frac{\sum_{k=1}^{N} L(\mathbf{x},\mathbf{y}_k)}{\sum_{k=1}^{N} L(\mathbf{x}_k,\mathbf{y})}\right\}$, set $\mathbf{y}_t \leftarrow \mathbf{y}$
  end for

distribution $Q(\mathbf{x}, \mathbf{y})$ that is chosen to be symmetric in order to relate the proposal weights directly to the likelihood function. This is attached to a Metropolis-within-Gibbs (MwG; Bai 2009) sampler for proposal draws. In total, it acts as an effective marginalization over the projection parameters for each shape parameter updates, leading to better mixing of the Markov chain and faster convergence overall.

Currently this method is publicly available in the `QuickCW` code (Bécsy et al. 2022). It has been shown to provide roughly a two-order-of-magnitude speed-up for the full CW Bayesian inference. The most recent NANOGrav CW analysis successfully utilized the `QuickCW` methods for efficiently searching the current 67-pulsar dataset (Agazie et al. 2023a).

3. Results

Considering the success of the `QuickCW` methods for CW searches from circular binaries, it is worth exploring if the same principles can be extended for a generalized CW searches of SMBHBs with varying eccentricity. Similar to Sec. 2.3, the induced signal can be divided into a series of coefficients and time-dependent basis functions:

$$s(t, \hat{\Omega}) = \sum_{j=1}^{6} \sigma_{6(i-1)+j}\left(\theta, \phi, \imath, \psi, \gamma_0, \Phi_0\right) S^{6(i-1)+j}(t) \tag{12}$$

where we see the inclusion of the initial angle of periapsis, γ_0, in the set of projection parameters, and note that the set of shape parameters present in the functions $S^{6(i-1)+j}$ adds in the mean anomaly, l, initial orbital eccentricity, e_0, and the mean frequency, F.

The exact forms of the coefficients and basis functions are contained within `GWecc` (Susobhanan et al. 2020; Susobhanan 2023), a PTA analysis code built exclusively for computing signals from eccentric SMBHB sources. This package is written using the Julia programming language to leverage just-in-time compilation for accelerating the code. Here we focus on the reformulated signal model present in the package, calculate a likelihood function that is separably by parameter class, customize an adaptive Metropolis sampler to perform the inference, and develop an MTMCMC routine to scale computational speed.

To test the performance of this new method, we generated two simulated datasets using the `libstempo` (Vallisneri 2020) code. Both datasets contained the same 45 pulsars present in the NANOGrav 12.5-year dataset with identical observing frequencies and TOA errors from the real data. We injected realistic white and red noise consistent with maximum likelihood values obtained from individual pulsar noise runs. In one dataset, we did not add any additional CW signal. For the other dataset we added a loud eccentric CW source with a effective signal amplitude roughly around $\log_{10} A \sim -6.5$, which corresponds to a ~ 100 ns delay contribution to the residuals. In total, we analyzed a 101-parameter model ($2 * N_{\rm psr}$ noise parameters, where $N_{\rm psr}$ is the number of pulsars in the array, and 11 parameters describing the SMBHB signal) with adaptive Metropolis sampling.

We first analyzed the dataset with no eccentric CW injection in an effort to calibrate the pipeline. Fig. 1 shows the one- and two-dimensional marginal distributions of a subset of signal parameters common amongst all the pulsars. The horizontal black lines denote the prior distributions on the parameters. All posteriors closely resemble their priors, which is indicative of a lack of a detection. The pipeline correctly finds that there is no CW present in the data, and as such the signal parameters are largely unconstrained. We note that despite the lack of an injection, the model appears to rule out the high-frequency and high-amplitude part of parameter space. This is likely due to the fact that binaries present in this extreme regime would experience noticeable frequency evolution over the observation time, and such evolution would be detectable if present.

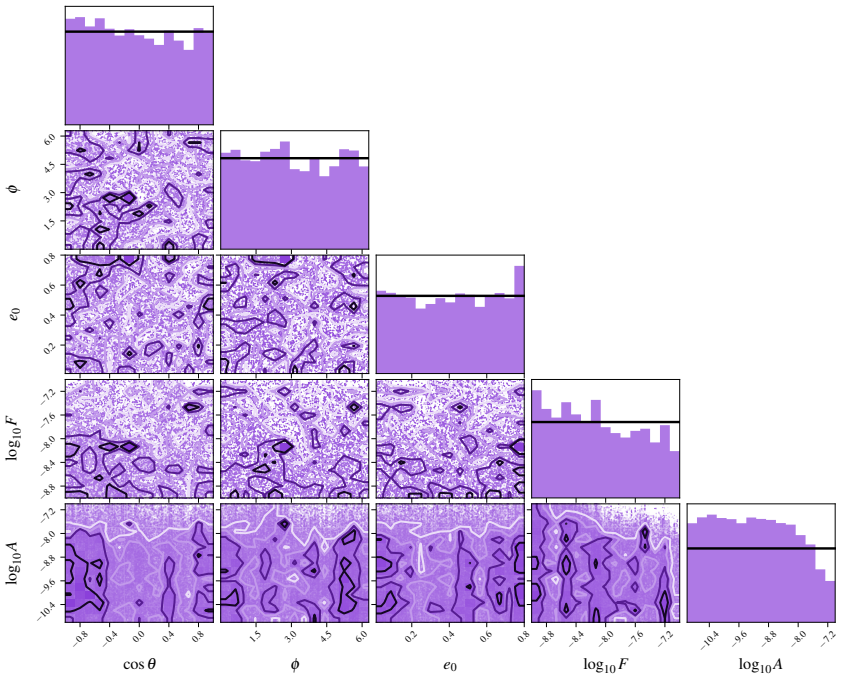

Figure 1: Corner plot of posterior distributions for a eccentric CW search, with a selection of parameters displayed being the source sky location (θ, ϕ) and intial eccentricity e_0, as well as the log mean frequency F and log effective signal amplitude $A \sim \mathcal{M}^{5/3}/d_L$. The analysis was run on a simulated dataset where no single source was injected. The posteriors accurately recover the absence of any signal, closely mirroring the uniform prior distributions denoted by the horizontal black lines.

Next we considered the case of a dataset with an eccentric CW present, one that is loud enough to be detectable given the data span. Fig. 2 displays the one- and two-dimensional distributions resulting from a search with the new pipeline. The black lines denote the injected parameter values. We correctly recover the CW signal, with all true values for the parameters falling largely within their respective posteriors. We note that in particular the frequency and amplitude are very well constrained respective to the width of their priors, owing again to the strength of the signal present.

Lastly, we tested the relative efficiency of the methods outlined above by directly comparing the likelihood evaluation wall times in the old pipeline and new MTMCMC routine. We ran this test on two simulated datasets. The first dataset was the loud CW injection datasets from above, and the other was double that dataset to allow us to scale the calculation times. For the old method we timed only the full likelihood calculation. For the method involving splitting into shape and projection parameters, we timed three separate instances of likelihood updates: one where only shape parameters were updated and others held fixed, one where projection parameters were updated and others fixed, and one where only the intrinsic pulsar red noise parameters were changed. The results are summarized in Table 1. We note that for fixed shape parameters the likelihood evaluation is nearly 20,000 times faster than the old likelihood. Even when considering all possible updates, the new computation is slightly faster, likely due to the speed-ups available through using Julia code. The shape parameter changes scale slightly faster than linearly with respect to the number of pulsars in the array, whereas projection parameter updates scale slightly slower than linearly.

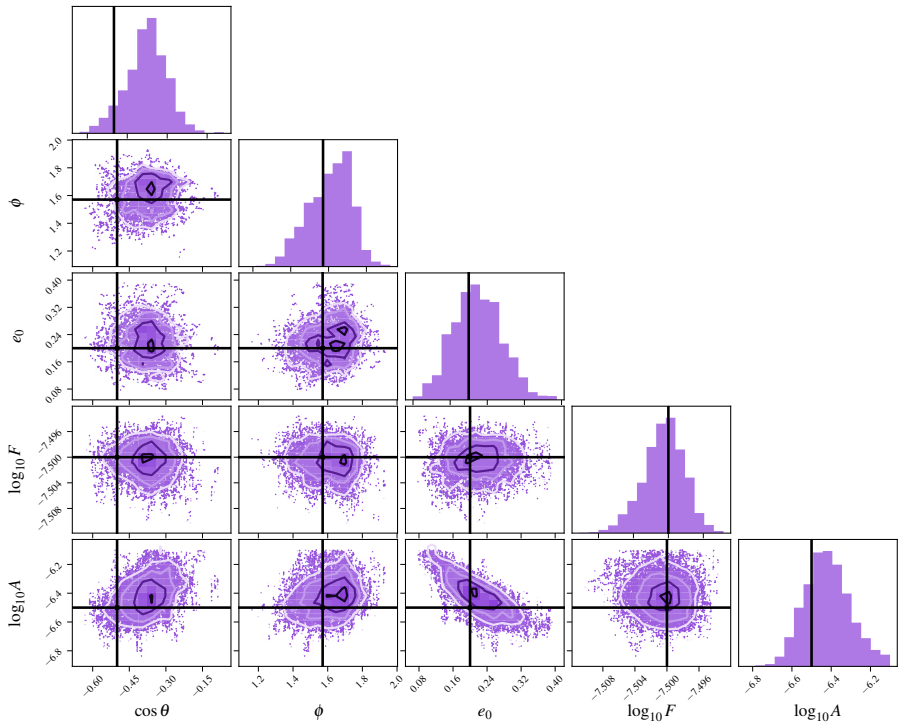

Figure 2: Corner plot of posterior distributions for an eccentric CW search run on a simulated dataset with a loud ($\log_{10} A \sim -6.5$) source injection. The selected parameters displayed here are the same as in Fig. 1. The signal is accurately recovered, with the injected parameters, denoted by black lines, falling well inside the posteriors.

	NANOGrav 12.5-year	2 x NANOGrav 12.5-year
# of pulsars	45	90
# of TOAs	410,064	820,128
Old likelihood calculation	9.5 ms	19.4 ms
Shape parameter update	2.8 ms	6.1 ms
Pulsar red noise update	4.0 ms	8.1 ms
Projection parameter update	0.5 μs	0.7 μs

Table 1: Comparison of evaluation wall times for old eccentric CW likelihood and reformulated likelihood parameter group updates. Wall times are shown for two datasets of varying size to show scaling of likelihood calculations.

4. Discussion

In this paper, we present a preliminary analysis for conducting fast Bayesian inference of GW signals from eccentric SMBHB orbits using PTA data. We find that by dividing the likelihood into two classes of parameters, shape and projection, and caching expensive inner products allow us to explore parts of parameter space more cheaply and numerously, which in total speeds up the full analysis over current techniques. This was shown using MTMCMC sampling techniques and tested through adaptive Metropolis sampling on two sets of simulated data.

With the discovery of a low-frequency GWB signal in hand, the focus of PTA collaboration research moves squarely into the realm of individual source detection and characterization. Having a fully general analysis pipeline will be crucial for detailed studies of these sources, their evolution, and their environments. This work, along with further merging of the methods of both the `QuickCW` and `GWecc` codes will prove useful towards furthering those goals and keeping the analyses running efficiently with ever-growing datasets.

We emphasize that the results outlined above used only simulated data, with idealized injection of white and red noise. Real PTA data will require broadening these methods to allow for a complete treatment of pulsar noise, described in detail in Agazie et al. (2023b), and will in turn prove more computationally burdensome. Also, in this paper we consider only one GW injection, that of an eccentric CW. Further development is required to perform these analyses while simultaneously marginalizing over the GWB parameters, or to deal with searches where multiple SMBHB sources can be jointly considered.

Acknowledgments

The NANOGrav project receives support from National Science Foundation (NSF) Physics Frontiers Center award number 1430284 and 2020265. This material is based upon work supported by NASA under Award No. RFP23_7-0 issued through Wisconsin Space Grant Consortium and the National Space Grant College and Fellowship Program, and any opinions, findings, and conclusions or recommendations expressed in this material are those of the authors and do not necessarily reflect the views of the National Aeronautics and Space Administration.

References

Agazie, G; et al. "The NANOGrav 15 yr Data Set: Bayesian Limits on Gravitational Waves from Individual Supermassive Black Hole Binaries," *ApJ*, v. 951(2), 2023a, p. L50. https://ui.adsabs.harvard.edu/abs/2023ApJ...951L..50A

Agazie, G; et al. "The NANOGrav 15 yr Data Set: Detector Characterization and Noise Budget," *ApJ*, v. 951(1), 2023b, p. L10. https://ui.adsabs.harvard.edu/abs/2023ApJ...951L..10A

Agazie, G; et al. "The NANOGrav 15 yr Data Set: Evidence for a Gravitational-wave Background," *ApJ*, v. 951(1), 2023c, p. L8. https://ui.adsabs.harvard.edu/abs/2023ApJ...951L...8A

Antoniadis, J; et al. "The second data release from the European Pulsar Timing Array III. Search for gravitational wave signals," *arXiv e-prints*, 2023, p. arXiv:2306.16214. https://ui.adsabs.harvard.edu/abs/2023arXiv230616214A

Armitage, PJ; Natarajan, P. "Eccentricity of Supermassive Black Hole Binaries Coalescing from Gas-rich Mergers," *ApJ*, v. 634(2), 2005, p. 921–927. https://ui.adsabs.harvard.edu/abs/2005ApJ...634..921A

Arzoumanian, Z; et al. "The NANOGrav 12.5 yr Data Set: Bayesian Limits on Gravitational Waves from Individual Supermassive Black Hole Binaries," *ApJ*, v. 951(2), 2023, p. L28. https://ui.adsabs.harvard.edu/abs/2023ApJ...951L..28A

Bai, Y. "An adaptive directional metropolis-within-gibbs algorithm", 2009

Bécsy, B; et al. "Fast Bayesian analysis of individual binaries in pulsar timing array data," *Phys. Rev. D*, v. 105(12), 2022, p. 122003. https://ui.adsabs.harvard.edu/abs/2022PhRvD.105l2003B

Charisi, M; et al. "Multimessenger time-domain signatures of supermassive black hole binaries," *MNRAS*, v. 510(4), 2022, p. 5929–5944. https://ui.adsabs.harvard.edu/abs/2022MNRAS.510.5929C

Detweiler, S. “Pulsar timing measurements and the search for gravitational waves,” *ApJ*, v. 234, 1979, p. 1100–1104. https://ui.adsabs.harvard.edu/abs/1979ApJ...234.1100D

Ellis, JA; Siemens, X; Creighton, JDE. “Optimal Strategies for Continuous Gravitational Wave Detection in Pulsar Timing Arrays,” *ApJ*, v. 756(2), 2012, p. 175. https://ui.adsabs.harvard.edu/abs/2012ApJ...756..175E

Foster, RS; Backer, DC. “Constructing a Pulsar Timing Array,” *ApJ*, v. 361, 1990, p. 300. https://ui.adsabs.harvard.edu/abs/1990ApJ...361..300F

Haiman, Z; et al. “The Population of Viscosity- and Gravitational Wave-driven Supermassive Black Hole Binaries Among Luminous Active Galactic Nuclei,” *ApJ*, v. 700(2), 2009, p. 1952–1969. https://ui.adsabs.harvard.edu/abs/2009ApJ...700.1952H

Hellings, RW; Downs, GS. “Upper limits on the isotropic gravitational radiation background from pulsar timing analysis.,” *ApJ*, v. 265, 1983, p. L39–L42. https://ui.adsabs.harvard.edu/abs/1983ApJ...265L..39H

Kormendy, J; Ho, LC. “Coevolution (Or Not) of Supermassive Black Holes and Host Galaxies,” *ARAA*, v. 51(1), 2013, p. 511–653. https://ui.adsabs.harvard.edu/abs/2013ARA&A..51..511K

Liu, J; Liang, F; Wong, W. “The multiple-try method and local optimization in metropolis sampling,” *Journal of The American Statistical Association - J AMER STATIST ASSN*, v. 95, 2000, p. 121–134

Metropolis, N; et al. “Equation of State Calculations by Fast Computing Machines,” *J. Chem. Phys.*, v. 21(6), 1953, p. 1087–1092. https://ui.adsabs.harvard.edu/abs/1953JChPh..21.1087M

Peters, PC. “Gravitational Radiation and the Motion of Two Point Masses,” *Physical Review*, v. 136(4B), 1964, p. 1224–1232. https://ui.adsabs.harvard.edu/abs/1964PhRv..136.1224P

Quinlan, GD. “The dynamical evolution of massive black hole binaries I. Hardening in a fixed stellar background,” *New Ast.*, v. 1(1), 1996, p. 35–56. https://ui.adsabs.harvard.edu/abs/1996NewA....1...35Q

Reardon, DJ; et al. “Search for an Isotropic Gravitational-wave Background with the Parkes Pulsar Timing Array,” *ApJ*, v. 951(1), 2023, p. L6. https://ui.adsabs.harvard.edu/abs/2023ApJ...951L...6R

Roedig, C; Sesana, A. “Origin and Implications of high eccentricities in massive black hole binaries at sub-pc scales,” In *Journal of Physics Conference Series*, v. 363 of *Journal of Physics Conference Series*, 2012, p. 012035. https://ui.adsabs.harvard.edu/abs/2012JPhCS.363a2035R

Sazhin, MV. “Opportunities for detecting ultralong gravitational waves,” *Soviet Ast.*, v. 22, 1978, p. 36–38. https://ui.adsabs.harvard.edu/abs/1978SvA....22...36S

Sesana, A; et al. “The Gravitational Wave Signal from Massive Black Hole Binaries and Its Contribution to the LISA Data Stream,” *ApJ*, v. 623(1), 2005, p. 23–30. https://ui.adsabs.harvard.edu/abs/2005ApJ...623...23S

Susobhanan, A. “Post-Newtonian-accurate pulsar timing array signals induced by inspiralling eccentric binaries: accuracy, computational cost, and single-pulsar search,” *Classical and Quantum Gravity*, v. 40(15), 2023, p. 155014. https://ui.adsabs.harvard.edu/abs/2023CQGra..40o5014S

Susobhanan, A; Gopakumar, A; Hobbs, G; Taylor, SR. “Pulsar timing array signals induced by black hole binaries in relativistic eccentric orbits,” *Phys. Rev. D*, v. 101(4), 2020, p. 043022. https://ui.adsabs.harvard.edu/abs/2020PhRvD.101d3022S

Taylor, SR; et al. “Detecting Eccentric Supermassive Black Hole Binaries with Pulsar Timing Arrays: Resolvable Source Strategies,” *ApJ*, v. 817(1), 2016, p. 70. https://ui.adsabs.harvard.edu/abs/2016ApJ...817...70T

Vallisneri, M. “libstempo: Python wrapper for Tempo2,” Astrophysics Source Code Library, record ascl:2002.017, 2020. https://ui.adsabs.harvard.edu/abs/2020ascl.soft02017V